Materials Horizons

ROYAL SOCIETY OF CHEMISTRY

COMMUNICATION

View Article Online
View Journal



Cite this: DOI: 10.1039/d5mh00578g

Received 31st March 2025,
Accepted 31st July 2025

DOI: 10.1039/d5mh00578g

rsc.li/materials-horizons



# Suppressing thermal degradation of $CsPbBr_3$ quantum dot/EVA films *via* APTES-mediated interface engineering: toward efficient and stable luminescence down-shifting for silicon solar cells

Hongfei Liang,[a] Lu Chen,[a] Yang Wu,[a] Youwen Xue,[b] Yuxuan Wang,[b] Wenjie Ji,[c] Huanqi Cao,[b] Qian Zhao,*[b] Jian Song *[a] and Guoran Li [c]

**Luminescence down-shifting technology is increasingly recognized as a crucial option for enhancing the efficiency of silicon solar cells. However, high-quality down-shifting materials, such as perovskite quantum dots, face challenges related to poor thermal stability. These materials tend to agglomerate into larger sizes, leading to the deterioration of the luminescence films at high temperature. Unlike introducing a protecting layer on perovskite quantum dots, we applied 3-aminopropyltriethoxysilane (APTES) as a direct capping agent for perovskite quantum dots in this work to achieve both efficient and stable composite down-shifting films. The interaction between APTES and $CsPbBr_3$ quantum dots is thoroughly analyzed using both experimental measurements and theoretical calculations. Due to the strong interaction between APTES and $CsPbBr_3$, an optimal amount of APTES effectively stabilizes the quantum dots. When mixed with ethylene-vinyl acetate (EVA) copolymer, the strong interaction between APTES and polymer chains could suppress the aggregation of $CsPbBr_3$ quantum dots and inhibit degradation of the composite film under heating. Upon coating on commercial crystalline silicon solar cells, the optimal $CsPbBr_3$ quantum dot/EVA composite film achieves an absolute efficiency by 1.00%, maintaining a 0.81% efficiency improvement even after annealing at 90 °C for 3 hours. In contrast, while the film without APTES shows an efficiency improvement of 0.63% at room temperature but experiences a decrease of 0.23% under the same heating conditions. This work provides a feasible strategy to enhance the thermal stability of $CsPbBr_3$ quantum dot/EVA composite films under high-temperature conditions, offering a promising path toward the commercial application of perovskite-based luminescence down-shifting films in silicon solar cells.**

[a] *School of Materials Science and Physics, China University of Mining and Technology, Xuzhou 221116, Jiangsu, China, jsoong@cumt.edu.cn*
[b] *School of Materials Science and Engineering, Tianjin University of Technology, Tianjin 300384, China, qian_zhao@email.tjut.edu.cn*
[c] *Institute of New Energy Materials Chemistry, School of Materials Science and Engineering, Nankai University, Tianjin 300350, China*

**New concepts**

This work demonstrates a novel strategy to enhance the thermal stability of $CsPbBr_3$ quantum dot (PQD)-based luminescence down-shifting (LDS) films for crystalline silicon solar cells by directly capping PQDs with 3-aminopropyltriethoxysilane (APTES). Unlike existing studies that focus on external encapsulation, APTES acts as a multifunctional interfacial agent, forming strong chemical bonds with both PQDs and the ethylene-vinyl acetate (EVA) polymer matrix. This dual interaction suppresses QD aggregation and film degradation under heat, addressing the critical instability issue of perovskite LDS materials. This new strategy can overcome the intrinsic limitations of perovskite nanomaterials, offering a scalable route for integrating unstable optoelectronic materials into solar cells.

## Introduction

Crystalline silicon solar cells, as the first commercially developed photovoltaic technology, have achieved a high level of technological maturity and currently dominate the global solar market with approximately 90% share. According to the spectral response curve of typical crystalline silicon cells, the photon conversion efficiency of the device exceeds 90% for light in the 500–800 nm wavelength range, but drops sharply to below 50% for wavelengths shorter than 500 nm.[1–5] Since there is a positive correlation between the spectral response and the photoelectric efficiency of solar cells, this indicates that crystalline silicon solar cells cannot effectively utilize the energy from ultraviolet and blue photons. Applying a film on the surface of traditional crystalline silicon solar cells that convert ultraviolet and blue light into lower-energy photons could significantly improve device efficiency at a low cost. This down-shifting technology holds great potential in the photovoltaic industry. All-inorganic perovskite $CsPbX_3$ (X = Cl, Br, I) quantum dots exhibit high photoluminescence quantum yields (PLQYs) of up to 90%, with an adjustable fluorescence wavelength spanning the entire visible spectrum. They also feature narrow emission linewidths, good defect tolerance, and grain size tunability through adjustment of the halogen precursor ratio or synthesis

conditions.[6–8] These properties make them promising candidates for down-shifting materials in silicon solar cells.

However, perovskite quantum dots are prone to surface anion exchange and are susceptible to decomposition under polar molecule exposure. They exhibit high sensitivity to environmental factors such as water vapor, light, and temperature, which limits their practical applications.[9–11] To improve the stability of perovskite quantum dots, various strategies have been explored, including metal/halide ion doping,[12] epitaxial growth,[13] surface ligand modification,[14–16] surface coating,[17–20] and composite formation with other materials.[21–23] Among these, inorganic silicon oxide coating is an effective strategy. For instance, Sun *et al.*[24] achieved the growth of $SiO_2$ thin shells on the surface of perovskite quantum dots through the adsorption of amino groups in 3-aminopropyltriethoxysilane (APTES) and the hydrolysis of silicon–oxygen bonds. Meng *et al.*[25] further improved this process by sequentially adding APTES, tetramethoxysilane (TMOS), and tetraethoxysilane (TEOS) to form a three-layer $SiO_2$ shell coating. Shi *et al.*[26] developed a triple silane coupling agent system for perovskite quantum dots, employing APTES, polydimethylsiloxane (PDMS), and hydrophilic siloxane-terminated polyethylene glycol (Si PEG) to form a protective shell while also enhancing water dispersibility. Li *et al.*[27] used pre-hydrolyzed TMOS for two-step modification to transform $Cs_4PbBr_6$ nanocrystals into $CsPbBr_3$ quantum dots while forming $SiO_x$ shells on their surfaces. The quantum dots obtained through this method have excellent monodispersity.

Integrating perovskite quantum dots into polymer matrices to form composite films represents a viable strategy of down-shifting in silicon solar cells. Our team prepared $CsPbBr_3$–$Cs_4PbBr_6$ perovskite quantum dot/ethylene-vinyl acetate (EVA) composite films, followed by surface modification of the quantum dots with diethyl zinc. As a down-shifting composite film for crystalline silicon solar cells, this approach achieved a 1.18% increase in the cell's power conversion efficiency.[28] Wang *et al.*[29] also demonstrated that an *in situ*-prepared $CsPbBr_3$ quantum dots/polyolefin elastomer (POE) adhesive film enhanced the power conversion efficiency (PCE) of crystalline silicon solar cells by 0.68% through hot pressing. This composite film fabrication approach could be compatible with existing photovoltaic adhesive film production lines. Although it is estimated to increase film costs by approximately 2–3 RMB $m^{-2}$ due to the use of perovskite quantum dots, a 1% efficiency enhancement for photovoltaic modules can be achieved. The resulting additional power generation revenue would fully cover the increased material cost.

However, due to the inherent temperature sensitivity of perovskite quantum dots and surface ligand desorption, polymers cannot fully protect the quantum dots from the damaging effects of moisture, heat, and oxygen. Consequently, the composite film is prone to degradation at elevated temperatures, manifesting as significant reductions in photoluminescence intensity and lifetime, as well as a diminished solar cell conversion efficiency. Given that the photovoltaic adhesive film will undergo a hot-pressing process and must also withstand the high temperatures generated during light exposure in the actual operation, protection of quantum dots is essential. Surface coating of perovskite quantum dots with inorganic oxides represents a reliable strategy to mitigate particle aggregation and growth within polymer matrices. However, such coatings may reduce the dispersibility of the perovskite quantum dots in solvents, and the oxides may not exclusively form on the surface of the quantum dots. The resulting scattered inorganic colloids could exhibit incompatibility with the polymer matrix, while the reduced dispersibility would compromise both the uniformity and transparency of the composite films. In this article, we propose a simple method to enhance the thermal stability of perovskite quantum dots using APTES. When combined with EVA, the resulting composite film exhibits excellent stability at 90 °C, effectively preventing degradation while significantly improving the efficiency of silicon solar cells.

## Materials and methods

### Materials

All chemical reagents were used as received without further purification, including cesium carbonate ($Cs_2CO_3$, 99.9%, Aladdin), lead bromide ($PbBr_2$, 99%, Aladdin), tetraheptylammonium bromide ($C_{28}H_{60}BrN$, 99%, Aladdin), oleic acid ($C_{18}H_{34}O_2$, 85%, Aladdin), octylamine ($C_8H_{19}N$, 99%, Aladdin), 1,2,4-trimethylbenzene ($C_8H_{12}$, 98%, Macklin), APTES ($C_9H_{23}NO_3Si$, 98%, Macklin), and ethylene vinyl acetate (EVA, Foster) copolymer. The multicrystal silicon solar cells were purchased from Anyang Guangke Jiao Energy Co., Ltd, with a size of $2 \times 2$ $cm^2$.

### Preparation of perovskite quantum dots/polymer composite films

0.0407 g of $Cs_2CO_3$ was stirred and dissolved in 2 mL of oleic acid (OA) at 70 °C, referred to as solution A. Next, 0.0588 g of $PbBr_2$, 0.1256 g of tetraheptylammonium bromide (TmBr), 160 μL of oleic acid, and 160 μL of octylamine (OLm) were added to 16 mL of 1,2,4-trimethylbenzene and stirred until fully dissolved, forming solution B. 200 μL of solution A was immediately injected into 2 mL of solution B, and the mixture was stirred on a hot plate at 70 °C and 500 rpm for 1.5 hours to prepare perovskite quantum dots. The solution was then centrifuged at 2000 rpm, and 3, 5, 10, 30, and 50 μL of APTES solution were added to every 1 mL of the supernatant, respectively. The mixture was heated at 70 °C and stirred at 500 rpm in air for 1 hour. Subsequently, 2 mL of EVA solution (0.1 g $mL^{-1}$ in 1,2,4-trimethylbenzene) was added to the mixture and stirred. To prepare the final composite film, 10 μL of different QD/EVA mixtures was spin-coated onto a solar cell at a speed of 1000 rpm. The film was then dried in an oven at 60 °C for 1 hour to yield a silicon solar cell with a downshifting composite film.

### Characterization

The fluorescence characteristics of the perovskite quantum dot composite films were analyzed using steady-state photoluminescence spectroscopy (PL, FS5, Edinburgh). The carrier lifetime of the composite films was measured using time-resolved

 

photoluminescence spectroscopy (TRPL, FLS980, Edinburgh). The composition, structure, and surface morphology of the materials were investigated through X-ray diffraction (XRD, D8 Advance, Bruker), field emission scanning electron microscopy (FESEM, SU8220, Hitachi), X-ray photoelectron spectroscopy (XPS, ESCALAB 250Xi, Thermo Fisher), and transmission electron microscopy (TEM, Tecnai G2 F20, FEI). The optical properties of the composite films were assessed using a UV-Vis spectrophotometer (UV-Vis, Cary 300, Varian). Additionally, Fourier-transform infrared spectroscopy (FT-IR, VERTEX 80 V, Bruker) was employed to identify specific functional groups in the polymer and composite films. The photovoltaic performance of silicon solar cells was evaluated by measuring the current density–voltage (*J–V*) characteristics using an electrochemical workstation (Keithley 2420 source meter), with the devices irradiated under standard AM1.5 simulated sunlight (100 mW $cm^{-2}$, Oriel Sol 3A, Newport). To accurately assess the performance of the composite film, we first measured the *J–V* curve of bare silicon solar cells and then compared it with those of pure polymer or varied perovskite quantum dots/composite films.

## Results and discussion

As shown in Scheme 1, there are usually two modification methods using APTES for the $CsPbBr_3$ perovskite quantum dots (in the following text, it is abbreviated as PQDs). One is to wash the surface ligand with ethyl acetate, then add APTES and hydrolyze it in air to obtain quantum dots with $SiO_x$ protection. However, the quantum dots obtained by this method have poor monodispersity and are prone to aggregation (Fig. S1a). Another approach is to directly add a controlled amount of APTES into the unpurified PQD solution. Due to the presence of other ligands such as oleic acid, even if APTES undergoes hydrolysis, it cannot undergo inward crosslinking to form a shell.[30]

Previous studies[31–33] have demonstrated that the PLQY of PQDs invariably decreases after purification, regardless of the solvent used, due to the removal of some surface ligands during the purification process, which facilitates aggregation and growth of quantum dots. However, since our quantum dots are intended for photoluminescence rather than electroluminescence, the presence of excessive free ligands does not impact the transparency of the solution. Consequently, omitting the purification step represents a viable strategy. The APTES reaction mechanism in solution is illustrated as follows,[25] where the Si–OH groups on APTES may undergo hydrolysis and crosslink with Si–OH groups on other APTES molecules, forming Si–O–Si bonds.

$$-NH_3^+ + X^- \rightarrow -NH_3X \quad (X = Br, I) \tag{1}$$

$$-SiOC_2H_5 + H_2O \rightarrow -SiOH + C_2H_5OH \tag{2}$$

$$-SiOH + -SiOC_2H_5 \rightarrow -SiOSi- + C_2H_5OH \tag{3}$$

$$-SiOH + -SiOH \rightarrow -SiOSi- + H_2O \tag{4}$$

To determine the phase composition of the PQDs, X-ray diffraction (XRD) analysis was conducted. As shown in Fig. 1, the prominent diffraction peaks of the PQDs match the standard reference patterns for $CsPbBr_3$. Specifically, peaks at 15.32°, 30.74°, and 44.57° correspond to the (110), (002), and (220) crystal planes of $CsPbBr_3$, respectively. When the APTES volume is below 10 μL, the peak positions and intensities remain identical to those of pristine PQDs, confirming that APTES addition at this level preserves the internal structure of $CsPbBr_3$ PQDs. However, at 30 μL APTES, new diffraction peaks emerge at 13.19° and 25.88°, indexed to the (110) and (024) planes of $Cs_4PbBr_6$, indicating the formation of a $CsPbBr_3$/$Cs_4PbBr_6$ composite phase localized at the PQD surface. With further increase of APTES volume to 50 μL, all $CsPbBr_3$-related peaks vanish, except the (220) peak at 44.57°. After annealing at 90 °C for 3 hours, the sharpened diffraction peaks suggest improved crystallinity for the pristine one. The PQD sample with ≤10 μL APTES maintains stable peak positions and intensities after annealing, demonstrating thermal stability in both phase composition and crystal size. In contrast, at 30 μL APTES, the $CsPbBr_3$ and $Cs_4PbBr_6$ peak intensities markedly decrease, accompanied by a new peak at 6° – evidence of APTES-induced ethanol hydrolysis driving perovskite transformation into a low-dimensional phase.[34] Additionally, the broad

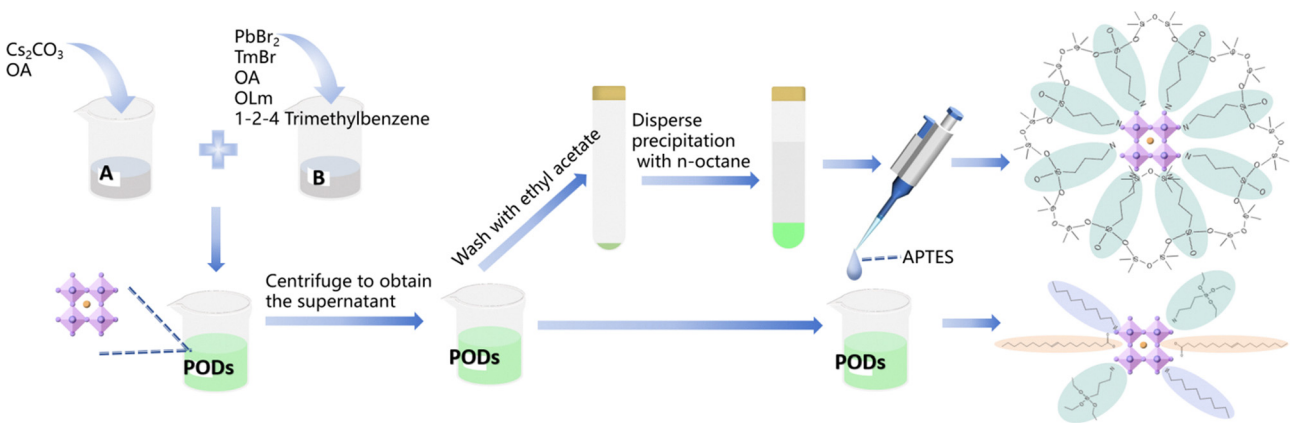


Scheme 1 Room temperature synthesis of $CsPbBr_3$ PQDs and two modification routes using APTES.

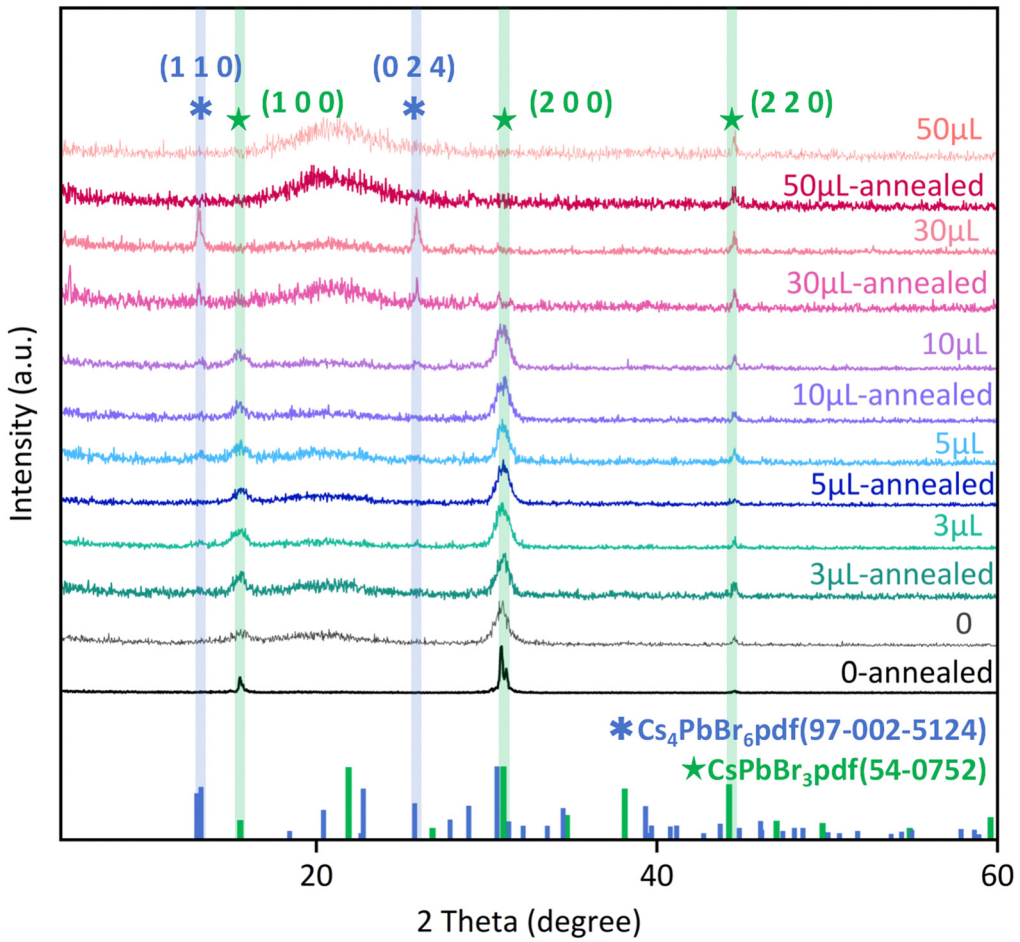


Fig. 1 XRD patterns of PQDs with different amounts of APTES before and after annealing at 90 °C for 3 h.

hump between 15° and 25° corresponds to amorphous $SiO_x$ derived from APTES (Fig. S1b).

In the transmission electron microscopy (TEM) image (Fig. 2a), the PQDs exhibit a uniform size distribution, with diameters ranging from 4 to 15 nm and an average size of 8.4 nm (Fig. S2a). As shown in Fig. 2b–d, the particle size showed a slight reduction, measuring approximately 7 nm (statistical data in Fig. S2b–d) with the addition of APTES amounts of 3, 5, and 10 μL. Generally speaking,[35,36] for perovskite quantum dots synthesized by room-temperature ligand-assisted methods, the stronger the electronegativity of the ligand or the greater the amount of ligand added, the smaller the resulting quantum dot size. According to our following computational simulations, the adsorption energy between APTES and $CsPbBr_3$ quantum dots is greater than that oleic acid and the quantum dots. Consequently, this inhibits the accumulation of $PbBr_2$ precursors on the quantum dot surface and suppresses the Ostwald ripening process. High-resolution TEM (Fig. 2e) reveals lattice fringes corresponding to the (110) and (200) planes of $CsPbBr_3$, as confirmed by interplanar spacing measurements. When the APTES concentration increases to 30 μL, the average particle size decreases to 2.6 nm (Fig. S2e), indicating ligand-induced size reduction, while micron-scale aggregates (~80 nm) emerge (Fig. 2f). At 50 μL APTES, isolated PQDs nearly disappear, leaving only large spherical particles (Fig. 2g). High-resolution TEM and energy-dispersive X-ray spectroscopy (EDS) mapping (Fig. S3) suggests these aggregates consist of $Cs_4PbBr_6$ and $SiO_x$, consistent with XRD analysis. Fig. 2h demonstrates significant coarsening of PQDs at elevated temperatures. Unmodified PQDs (Fig. 2a) follow isotropic Ostwald ripening,[37] where ions dissociate from smaller grains and redeposit on larger ones, a process accelerated by temperature. In APTES-modified samples (Fig. 2i), amino groups passivate surface defects *via* adsorption, while outward-oriented organic chains and Si–O bonds reduce interparticle forces, effectively suppressing thermal coarsening. Elemental mapping (Fig. S4) confirms uniform distributions of Cs, Pb, and Br in PQDs/EVA films pre- and post-annealing. The APTES-modified PQDs/EVA film additionally shows homogeneous Si distribution, further verifying its thermal stability.

The X-ray photoelectron spectroscopy (XPS) results shown in Fig. 3 characterize the valence states of the pristine PQDs, APTES-modified PQDs (PQDs@APTES), and PQDs@APTES/EVA composite films. As shown in Fig. 3a, all the samples exhibit characteristic peaks for Cs, Pb, Br, C, N, and O. The incorporation of APTES allows for the detection of the Si element in both PQDs@APTES and PQDs@APTES/EVA composite films. The perovskite quantum dots display two emission peaks (Fig. 3b), corresponding to Pb $4f_{5/2}$ and Pb $4f_{7/2}$. After

 

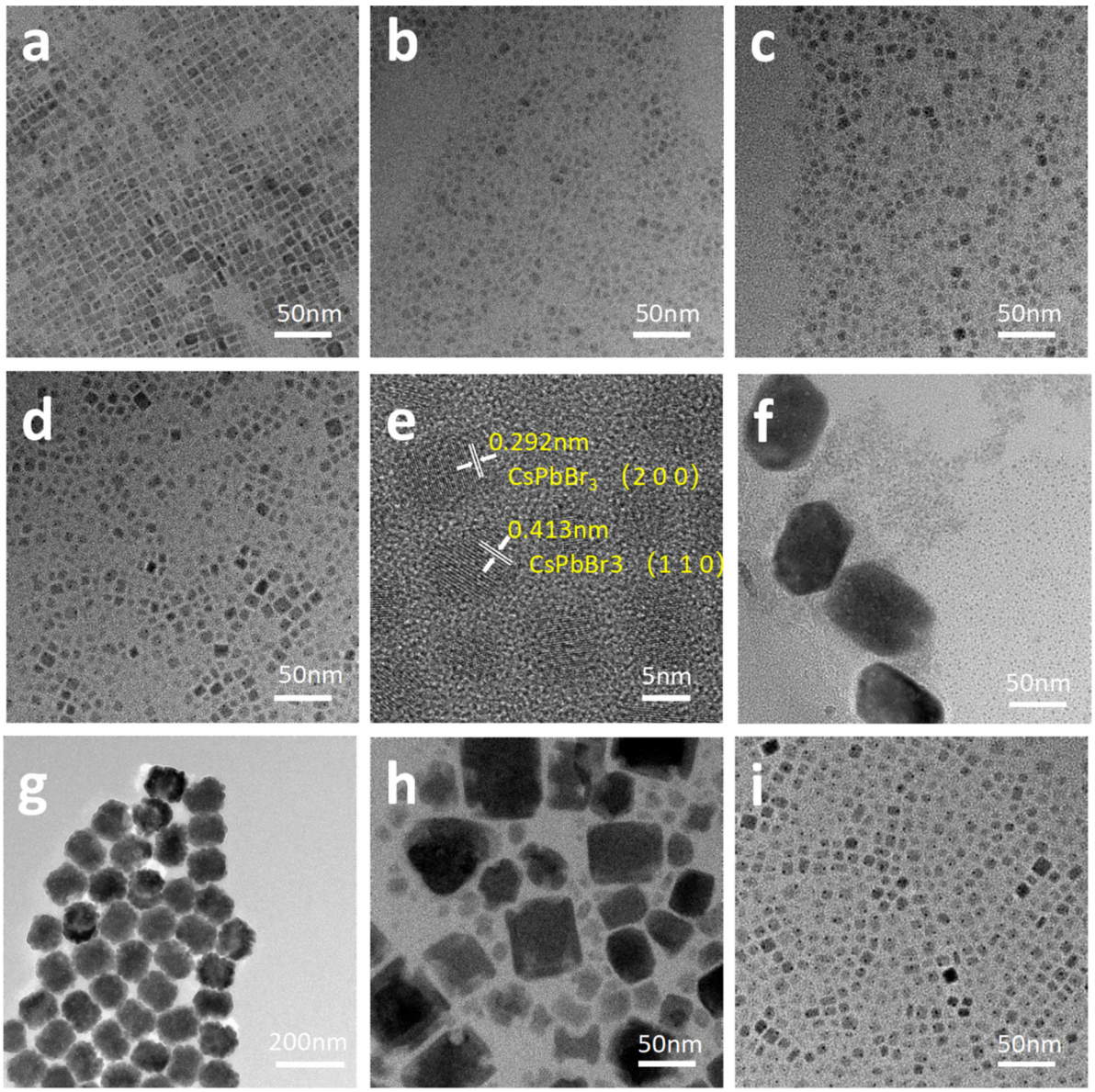


Fig. 2 TEM images of (a) PQDs and PQDs with (b) 3 μL mL$^{-1}$, (c) 5 μL mL$^{-1}$, (d) 10 μL mL$^{-1}$, (f) 30 μL mL$^{-1}$, and (g) 50 μL mL$^{-1}$ APTES. TEM images of PQDs (h) without and (i) with 10 μL APTES/mL after being heated at 90 °C for 3 h. (e) High resolution TEM images of PQDs modified with 10 μL mL$^{-1}$ APTES.

modification with APTES, these peaks shift to 142.39 eV and 137.54 eV, respectively, compared to the PQDs. In Fig. 3c, for the Br 3d spectrum, the peaks at 68.59 eV and 67.54 eV correspond to Br $3d_{3/2}$ and Br $3d_{5/2}$, respectively. These peaks shift to 68.49 eV and 67.44 eV after modification, with both binding energies decreasing by 0.1 eV. This reduction in binding energy suggests a weakened Pb–Br bond, which conforms to the common rules of cationic ligands.[38] However, the higher binding energies observed for the pristine quantum dots likely originate from aggregation and growth of the quantum dots during the drying process of sample preparation. In contrast, the quantum dots maintain their original morphology after modification with APTES. Upon mixing with EVA, both Pb $4f_{5/2}$ and Pb $4f_{7/2}$ peaks shift to higher binding energies in the composite film, indicating a more stable structure,[39–41] while the Br $3d_{3/2}$ and Br $3d_{5/2}$ peaks show little change. In Fig. 3d, a peak at 101.84 eV is observed, corresponding to the Si–O bond. This peak is absent in the original PQDs' spectrum, indicating the adsorption of APTES onto the surface of the quantum dots.

Fourier transform infrared spectroscopy (FT-IR) was used to analyze the functional groups present in different samples, as shown in Fig. 4a. The pristine quantum dots exhibit a symmetric stretching vibration of the carboxylic acid (COOH) group from oleic acid at 1708 cm$^{-1}$, along with C–H stretching vibrations at 1548, 2921 and 2850 cm$^{-1}$, which are characteristic of organic ligands such as oleic acid and octylamine.[42] In contrast, due to the existence of APTES, the attenuation of these peaks confirms partial ligand substitution. When the modified quantum dots are mixed with EVA, the FT-IR spectrum reveals peaks at 1735 cm$^{-1}$ and 1236 cm$^{-1}$, which correspond to the

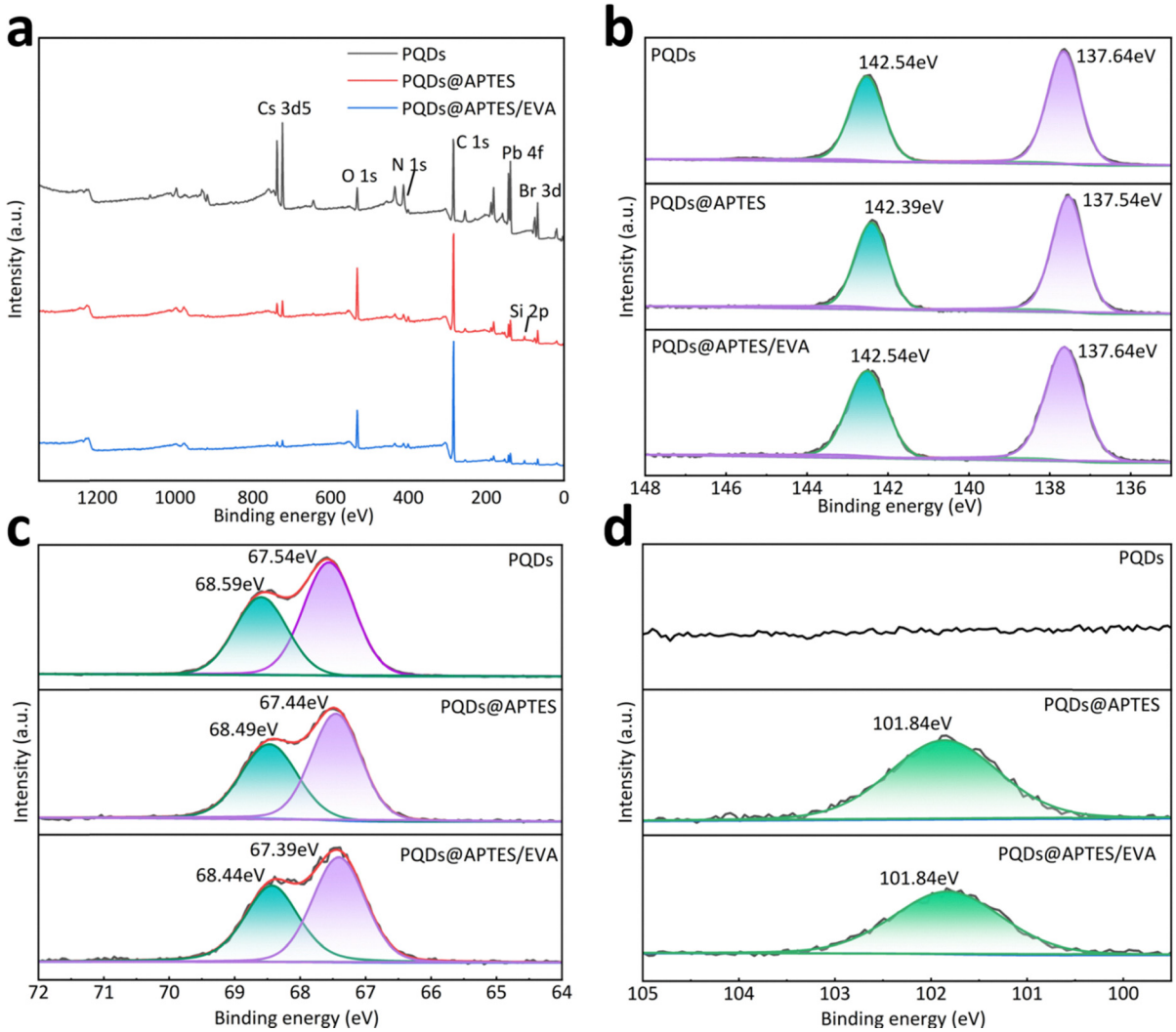


Fig. 3 (a) Wide-scan XPS spectra of PQDs, PQDs/EVA and PQDs@APTES (10μL $mL^{-1}$)/EVA, and narrow-scan XPS spectra of (b) Pb 4f, (c) Br 3d, and (d) Si 2p of different films.

C═O and C–O–C bonds in EVA. Other peaks at 2916 $cm^{-1}$, 2848 $cm^{-1}$, 1020 $cm^{-1}$, and 719 $cm^{-1}$ are attributed to the stretching vibrations of C–H and C–O bonds in EVA.[43] The peak at 1544 $cm^{-1}$ corresponds to the N–H bending vibration from APTES.[44] The spectrum of $SiO_x$ formed by the natural hydrolysis of pure APTES in air is also presented in Fig. 4. The peaks at 1001 $cm^{-1}$ and 686 $cm^{-1}$ can be attributed to Si–O–Si, which exhibit a red-shift compared with the peak at 1130 $cm^{-1}$, indicating that the Si–O–Si bond energy in naturally hydrolyzed APTES is low, forming a loose network structure.[44]

Due to the fact that the outer surface of $CsPbBr_3$ is Br-rich under realistic conditions,[45] we selected the (−1 0 0) surface and removed Cs atoms to obtain a Br-terminated surface. As shown in Fig. S5a, the bridge site between two Pb atoms exhibits a positively charged region, while the N atom in APTES is surrounded by a negatively charged region (Fig. S5b). Therefore, the adsorption of APTES at the Pb bridge site is theoretically feasible. Then we determined the adsorption energy of oleic acid (OA) and APTES on the quantum dot surfaces and their interactions with EVA molecules by density functional theory (DFT) calculations (The Calculation section is in the SI). As shown in Fig. 4b, $CsPbBr_3$ exhibits a lower adsorption energy with oleic acid (−0.01 eV) and a higher adsorption energy with APTES (−0.76 eV). The results demonstrate that APTES can function as a dual-functional surface modifier for $CsPbBr_3$ quantum dots, effectively passivating surface defects through vacancy filling while demonstrating ligand exchange capability to partially displace OA molecules. The higher adsorption energy significantly reduces the detachment risk of the ligand on PQDs, which could restrain aggregation of quantum dots during film fabrication. The adsorption energy of APTES and EVA (−0.94 eV) is also stronger than that of OA (−0.11 eV), indicating that PQDs with the APTES capping agent could have a higher solubility in EVA. This is a critical prerequisite to obtain a composite film with good transparency.

For an effective $CsPbBr_3$ green down-shifting film for silicon solar cells, it should exhibit high light transmission in the 500–800 nm wavelength range and strong light absorption in the

 

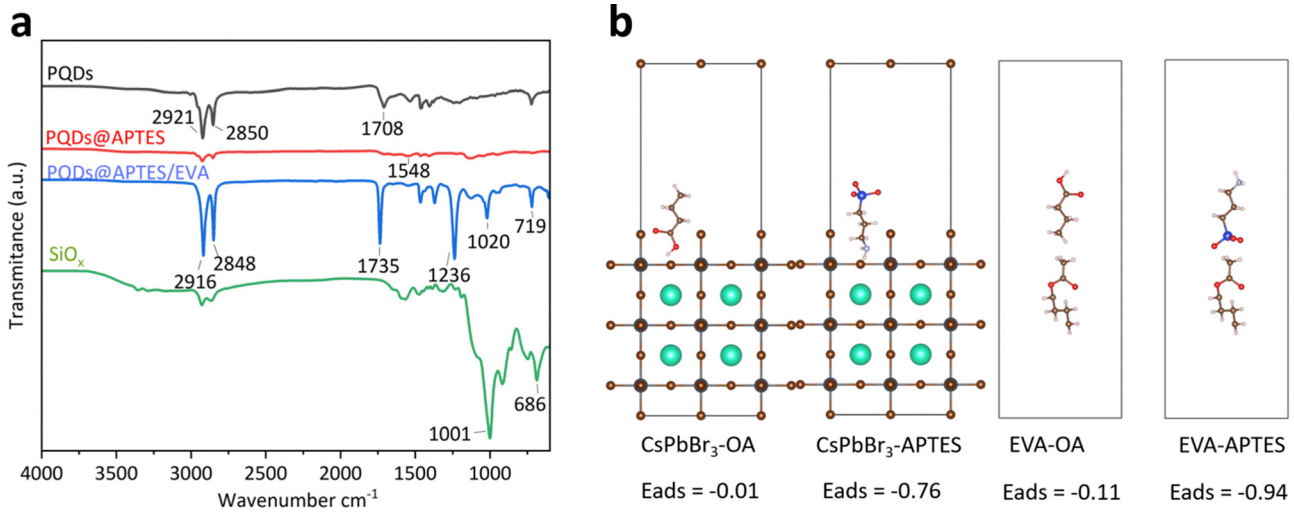


Fig. 4 (a) FT-IR spectra of PQDs, PQDs@APTES (10μL mL$^{-1}$), PQDs@APTES/EVA and $SiO_x$ prepared using pure APTES in air. (b) The adsorption energy calculation results of $CsPbBr_3$ with OA and APTES, EVA with OA and APTES.

200–500 nm range to ensure optimal photovoltaic performance. From Fig. 5a, it can be observed that the pristine PQDs/EVA composite film shows low light transmission below 500 nm, indicating good light absorption by the perovskite quantum dots. However, light transmission above 500 nm is also quite low, which will limit the photon utilization in silicon solar cells. Upon the introduction of APTES, a smaller particle size and better dispersivity in EVA benefits light transmission of the films. Therefore, the addition of APTES improves light transmission at longer wavelengths, but the phase conversion of perovskite quantum dots adversely affects their light absorption at shorter wavelengths. A balance must be struck between enhancing light transmission at longer wavelengths and maintaining light absorption at shorter wavelengths. The pristine PQDs/EVA composite film after annealing at 90 °C for 3 hours shows improved light transmission above 500 nm, which could be attributed to the aggregation and growth of the PQDs. The reduction in the number of PQDs leads to a decrease in light scattering. This improvement is not what we expected, as its ability to absorb and convert short wavelength light has decreased. While PQDs/EVA composite films with 3, 5, and 10 μL APTES maintain their light transmission performance after annealing, demonstrating the protective effect of APTES on the perovskite quantum dots. For the film with 30 μL APTES, the enhanced light transmission can be attributed to the transformation of the perovskite structure into a low-dimensional phase at higher temperatures, as confirmed by the XRD results.

The photoluminescence (PL) properties of the different films are shown in Fig. 5b. When 3 μL of APTES is added, the PL intensity of the composite film slightly decreases compared to the pristine PQDs/EVA composite film, while as more APTES is introduced (5–10 μL), the PL intensity gradually increases and becomes comparable to that of the pristine film, which can be attributed to the surface passivation and protection provided by APTES. On the other hand, when the APTES amount reaches 30 μL or more, the peak intensity sharply decreases, likely due to the decomposition of the perovskite quantum dots under excess APTES. After annealing at 90 °C for 3 hours, the peak of the pristine PQDs/EVA composite film shifts from 512 nm to 526 nm, with the peak intensity dropping to only 3% of its initial value before annealing. The optimal performance is observed in the PQDs/EVA composite film with 10 μL APTES, which shows a slight increase in the full-width at half maximum (FWHM), while the peak intensity remains at 78% of its original value before annealing. Meanwhile, the PLQY of the PQDs@APTES/EVA composite film has increased from 66.07% to 94.05% compared to the PQDs/EVA composite film (Fig. 5c). These results suggest that the addition of APTES effectively preserves the fluorescence performance of the quantum dots.

Transient time-resolved photoluminescence (TRPL) spectroscopy was conducted (Fig. 5d), and the TRPL decay curves were fitted using a double exponential decay function, which included two decay components. The decay times, $\tau_1$ and $\tau_2$, correspond to non-radiative recombination and intrinsic radiation recombination of charge carriers, respectively.[46] The fluorescence lifetime of PQDs/EVA composite films with a small amount of APTES added is generally around 12 ns (Table S1), which is approximately 5 ns longer than that of the pristine PQDs/EVA composite film. This indicates that APTES helps passivate the surface defects of the quantum dots. However, when the APTES concentration exceeds 30 μL, the quantum dots begin to decompose, leading to a significant reduction in the fluorescence lifetime. After annealing at 90 °C for 3 hours, the pristine PQDs/EVA composite film loses its photoluminescent properties, resulting in the fluorescence lifetime approaching zero. In contrast, the fluorescence lifetime of the PQDs/EVA composite films with a small amount of APTES remains stable at around 9–10 ns (Table S2). This indicates that APTES effectively passivates surface defects on the quantum dots and helps maintain their performance even at elevated temperature.

To rigorously evaluate the photovoltaic performance enhancement provided by these down-shifting composite films

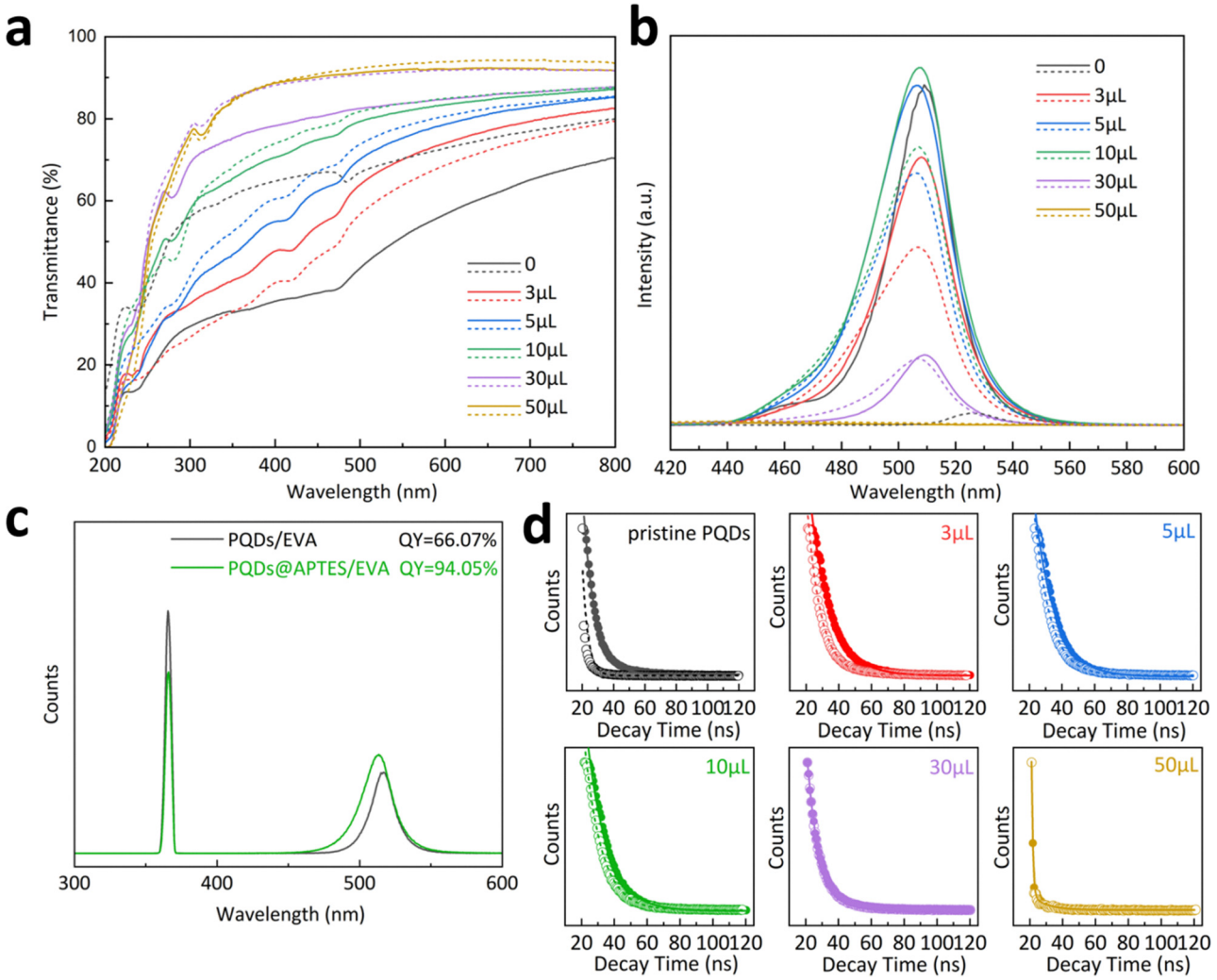


Fig. 5 (a) The UV-Vis spectra and (b) PL spectra of PQDs/EVA composite films before (solid line) and after (dashed line) annealing at 90 °C for 3 h. (c) PLQY diagram of the PQD/EVA composite film and the PQDs@APTES (10 μL $mL^{-1}$)/EVA composite film. (d) TRPL spectra of PQDs/EVA composite films before (solid spheres) and after (hollow spheres) annealing.

and their tolerance at high temperatures, we first tested a bare silicon solar cell, referred to as the reference device. Next, we spin-coated 10 μL of different QD/EVA mixtures onto the same solar cell at a speed of 1000 rpm and then measured its device performance. Finally, we subjected the device to annealing at 90 °C for 3 hours and evaluated its photovoltaic performance. All three tests were based on the same reference device. Therefore, any efficiency changes observed in the device with the down-shifting film can be attributed to the coating film rather than the silicon solar cell itself. As shown in Fig. 6a–e and Table 1, all of the perovskite quantum dot composite film coatings improved the efficiency of the solar cells. The efficiency enhancement is mainly attributed to the improvement of $J_{sc}$, originating from spectral conversion of quantum dots.[47] Parallel test results are shown in Table S3, and the average PCE improvement was calculated and is shown in Fig. 6f. We observe that the best performance was achieved with 10 μL of APTES, resulting in an efficiency increase of 1.00% (0.80% on average), significantly higher than 0.63% (0.37% on average) obtained using the pristine PQDs/EVA composite film. The device efficiencies are close to the 13.73% absolute efficiency achieved by the Abdelbar team.[48] The relatively low values could originate from the downsizing process for small-sized crystalline silicon solar cells, which might induce microstructural defects including microcracks and elevated interfacial contact resistance, potentially compromising device performance relative to standard commercial modules. After annealing at 90 °C, the efficiency of the devices generally decreased. For the pristine PQDs/EVA, the efficiency even decreased by 0.23% (0.11% on average) compared to the reference device. However, the devices with APTES-modified PQDs/EVA composite films still exhibited enhanced efficiency compared to the reference. The optimal performance was still observed with the 10 μL APTES film, with an efficiency increase of 0.81% (0.68% on average) compared to the reference device, although this was a small decrease compared to the non-annealed device.

Based on the characterization results of composite films before and after annealing, it was found that a concentration of

 

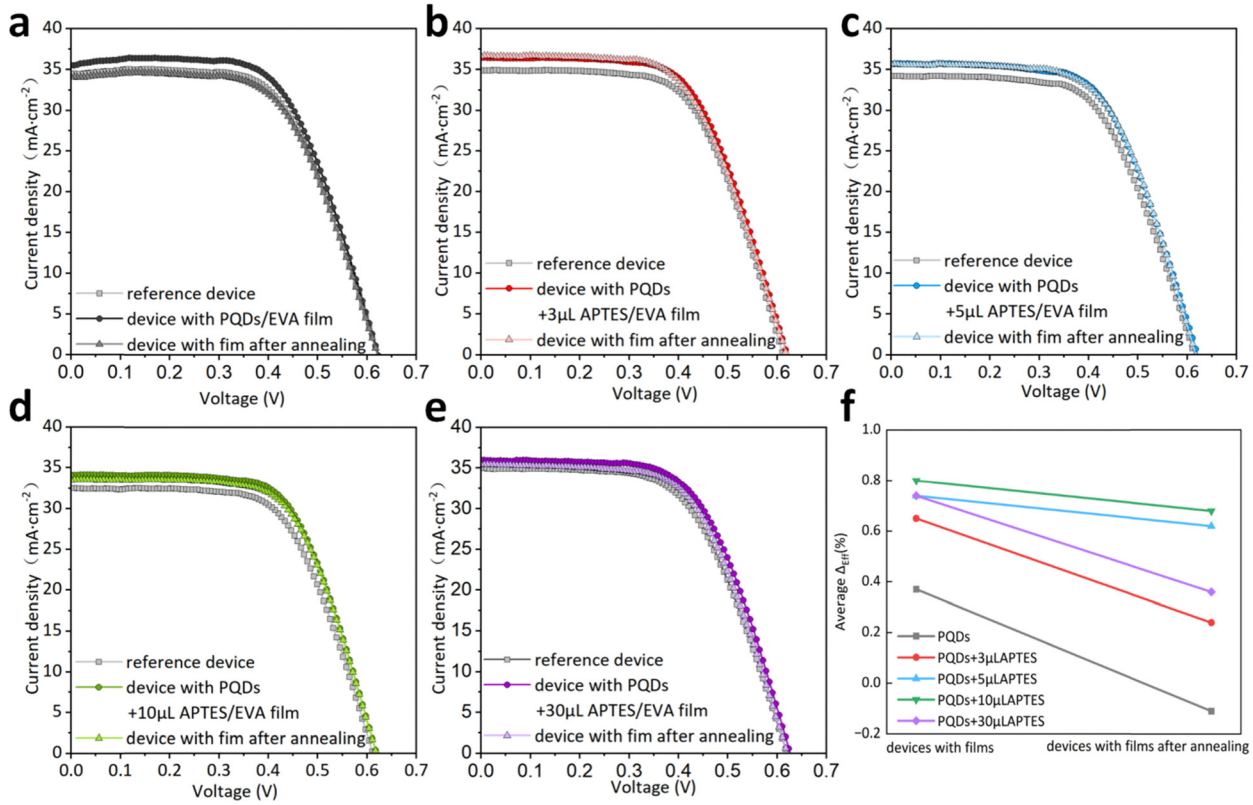


Fig. 6 *J*–*V* curves of silicon solar cells using (a) PQDs/EVA, (b) PQDs with 3 μL APTES/EVA, (c) PQDs with 5 μL APTES/EVA, (d) PQDs with 10 μL APTES/EVA, and (e) PQDs with 30 μL APTES/EVA. (f) Average value of $\Delta_{Eff}$ (%) for devices with different composite films.

Table 1 The photovoltaic parameters of devices with different composite films

| | Reference devices | | | | Devices with composite films | | | | | Devices with composite films beyond 90 °C | | | | |
|---|---|---|---|---|---|---|---|---|---|---|---|---|---|---|
| | $V_{oc}$ (V) | $J_{sc}$ (mA cm$^{-2}$) | FF (%) | PCE (%) | $V_{oc}$ (V) | $J_{sc}$ (mA cm$^{-2}$) | FF (%) | PCE (%) | $\Delta_{Eff}$ (%) | $V_{oc}$ (V) | $J_{sc}$ (mA cm$^{-2}$) | FF (%) | PCE (%) | $\Delta_{Eff}$ (%) |
| Pristine PQDs | 0.62 | 34.49 | 61.53 | 13.21 | 0.62 | 35.66 | 62.28 | 13.84 | 0.63 | 0.62 | 34.08 | 61.28 | 12.98 | −0.23 |
| 3 μL APTES | 0.61 | 34.38 | 62.63 | 13.21 | 0.62 | 35.80 | 62.53 | 13.92 | 0.70 | 0.62 | 36.23 | 60.66 | 13.62 | 0.41 |
| 5 μL APTES | 0.62 | 33.76 | 61.20 | 12.75 | 0.62 | 35.05 | 62.17 | 13.55 | 0.80 | 0.62 | 35.04 | 61.91 | 13.39 | 0.64 |
| 10 μL APTES | 0.61 | 32.00 | 63.88 | 12.54 | 0.62 | 33.59 | 64.96 | 13.54 | 1.00 | 0.62 | 33.00 | 65.20 | 13.35 | 0.81 |
| 30 μL APTES | 0.61 | 33.84 | 61.18 | 12.67 | 0.62 | 35.18 | 61.94 | 13.53 | 0.86 | 0.62 | 33.70 | 62.86 | 13.06 | 0.22 |

10 μL mL$^{-1}$ APTES additive appeared to be optimal. Therefore, to explore the composite film performance under more stringent conditions, the 10 μL mL$^{-1}$ APTES concentration was selected for the experimental group. As shown in Fig. 7a and b, for the pristine PQDs/EVA composite films, the PL peaks almost disappeared after 1 hour of annealing at 140 °C. This indicates that pristine $CsPbBr_3$ PQDs could not withstand the common photovoltaic adhesive encapsulation temperatures encountered in industrial production. In contrast, the APTES-modified PQDs/EVA composite films retained approximately 75% of their initial fluorescence intensity. For the films subjected to UV exposure (Fig. 7c and d), the pristine PQDs/EVA composite films exhibited weakened and asymmetric fluorescence. As reported,[49] $CsPbBr_3$ undergoes photodegradation under light, where $Br^-$ ion dissociation leads to aggregation, defect formation, and trap states. APTES modification significantly suppressed this degradation trend. Regarding water immersion (Fig. 7e and f), although the perovskite is inherently sensitive to moisture,[50] the EVA encapsulation effectively prevented water molecule penetration into the composite film. Consequently, no significant fluorescence quenching was observed upon water immersion.

The operational stability of silicon solar cells coated with either PQD/EVA or PQDs@APTES (10μL)/EVA was also evaluated under continuous illumination and heating (Fig. 8). After 192 hours of illumination, the device efficiency increased by only 0.32% for PQD/EVA, compared to a 0.73% increase for the PQDs@APTES/EVA device. Similarly, after 192 hours of continuous heating, the efficiency decreased by 0.24% for PQD/EVA, whereas the PQDs@APTES/EVA device exhibited a 0.58% increase. These results further confirm the enhanced thermal stability and photostability imparted by APTES modification to the composite films.

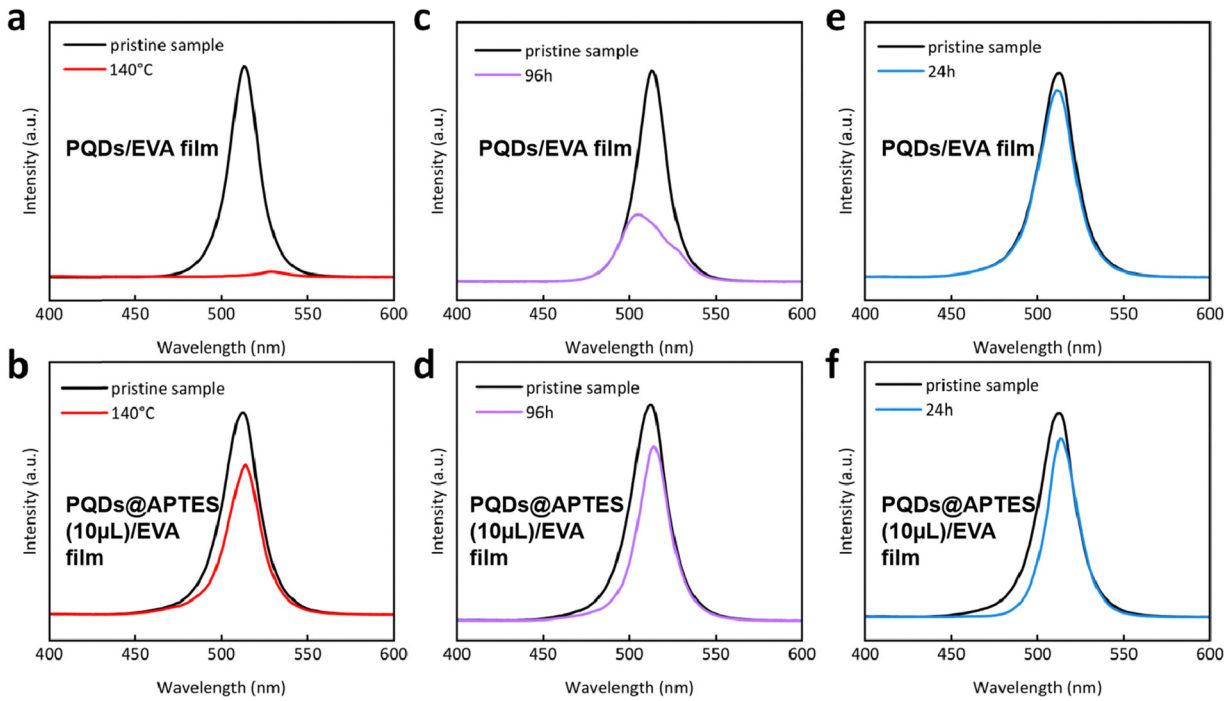


Fig. 7 PL spectra of PQDs/EVA and PQDs@APTES (10 μL)/EVA composite films after (a) and (b) annealing at 140 °C for 1 hour, (c) and (d) illumination with a 365 nm UV light lamp with a power of 100 W for 96 h, and (e) and (f) soaking in water for 24 h.

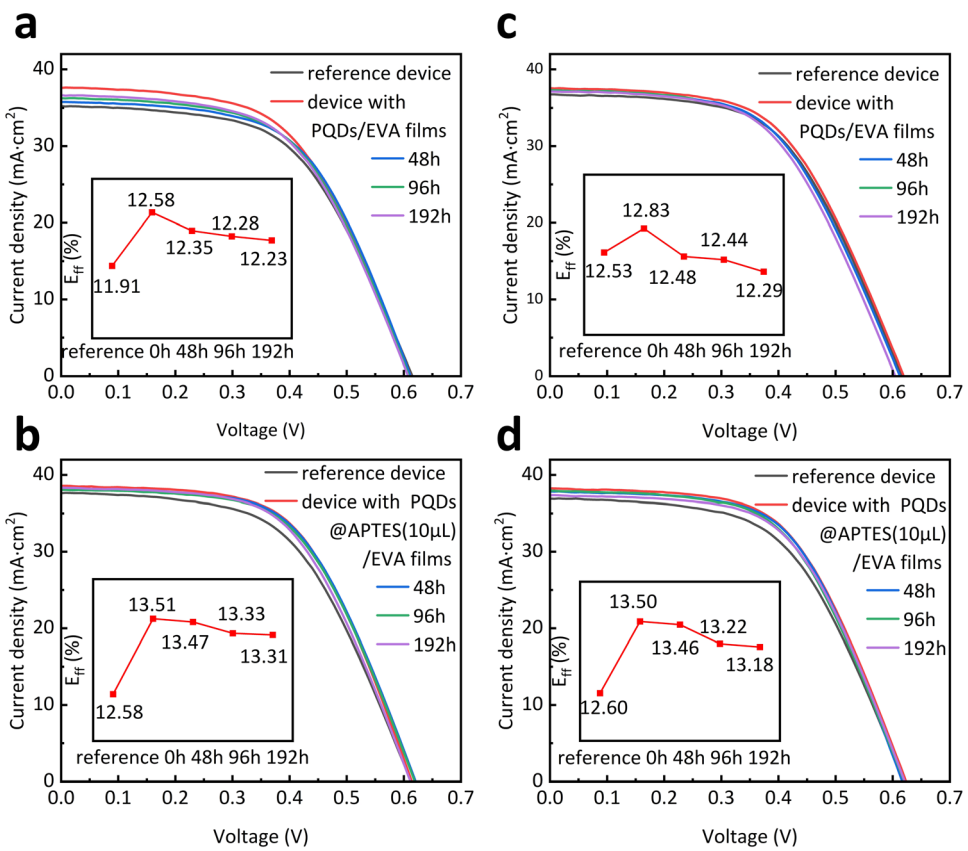


Fig. 8 *J*–*V* curves of silicon solar cells working under standard sunlight for different times using (a) PQDs/EVA and (b) PQDs@APTES (10 μL)/EVA. *J*–*V* curves of silicon solar cells working at 90 °C for different times using (c) PQDs/EVA and (d) PQDs@APTES (10 μL)/EVA.

 

## Conclusions

In this study, we successfully developed a composite luminescence down-shifting film with both high efficiency and exceptional thermal stability by employing 3-aminopropyltriethoxysilane (APTES) as a direct capping agent for $CsPbBr_3$ perovskite quantum dots. Experimental characterization and theoretical calculations revealed that the strong interaction between APTES and $CsPbBr_3$ PQDs effectively suppressed PQD aggregation under high-temperature conditions. Simultaneously, the robust bonding between APTES and ethylene-vinyl acetate (EVA) copolymer chains increases the transparency of the composite film. When applied to commercial crystalline silicon solar cells, the optimized $CsPbBr_3$ PQD/EVA composite film achieved an absolute efficiency enhancement of 1.00%, retaining a 0.81% improvement even after annealing at 90 °C for 3 hours. In contrast, the film without APTES exhibited a reduced efficiency under identical heating conditions, underscoring the critical role of APTES in stabilizing the PQDs. The composite film modified by APTES also presented better performance under more stringent conditions, such as high temperature, moisture, UV light, and long-term illumination/heating. This work provides a reliable solution to improve the high-temperature stability of PQD-based down-shifting films and validate their practical application potential in commercial silicon solar cells, opening a promising avenue for advancing photovoltaic efficiency through stable and scalable luminescence down-shifting technologies.

## Author contributions

Hongfei Liang: conceptualization, investigation, writing – original draft. Lu Chen: software, visualization. Yang Wu, Youwen Xue, Yuxuan Wang, and Wenjie Ji: investigation, data curation. Huanqi Cao: writing – review & editing. Qian Zhao, Jian Song, and Guoran Li: project administration, supervision, writing – review & editing, funding acquisition. All the authors reviewed the manuscript.

## Conflicts of interest

There are no conflicts to declare.

## Data availability

The data that support the findings of this study are available within the manuscript and the SI. The raw data files acquired from the instruments or noted by hand in laboratory books are available in numerical form from the authors.

Supplementary information is available. See DOI: **https://doi.org/10.1039/d5mh00578g**

## Acknowledgements

We appreciate the financial support from the National Natural Science Foundation of China (52203369) and the Tianjin Natural Science Foundation (24JCQNJC00960).

## References

1 J. Nelson, *The physics of solar cell, London*, Imperial College Press, 2003, pp. 67–161.
2 R. L. Crabb, Photon induced degradation of electron and proton irradiated silicon solar cells, *IEEE Trans. Nucl. Sci.*, 1973, **20**, 243–249.
3 International Energy Agency. Renewable 2022 Analysis and forecast to 2027. Paris: IEA, 2022, pp. 54–56.
4 D. Dong, X. D. Da and Q. Cheng, Application of dual-layer poly silicon deposited by PECVD in n-type TOPCon solar cells, *Sol. Energy Mater. Sol. Cells*, 2023, **261**, 112.
5 M. Nakamura, M. Yamaguchi and K. Kimoto, *et al.*, Cd free Cu(In, Ga)(Se, S)2 thin-film solar cell with record efficiency of 23.35%, *IEEE J. Photovolt.*, 2019, **9**, 1863–1867.
6 L. Protesescu, S. Yakunin and M. I. Bodnarchuk, *et al.*, Nanocrystals of cesium lead halide perovskites($CsPbX_3$, X = Cl, Br, and I): novel optoelectronic materials showing bright emission with wide color gamut, *Nano Lett.*, 2015, **15**, 3692–3696.
7 L. Xu, J. Li and T. Fang, *et al.*, Synthesis of stable and phase-adjustable $CsPbBr_3$@$Cs_4PbBr_6$ nanocrystals via novel anion-cation reaction, *Nanoscale Adv.*, 2019, **1**, 980–988.
8 S. Panigrahi, S. Jana and T. Calmeiro, *et al.*, Imaging the anomalous charge distribution inside $CsPbBr_3$ perovskite quantum dots sensitized solar cell, *ACS Nano*, 2017, **11**, 10214–10221.
9 Y. Huang, W. Luan and M. Liu, *et al.*, DDAB-assisted synthesis of iodine-rich $CsPbI_3$ perovskite nanocrystals with improved stability in multiple environments, *J. Mater. Chem. C*, 2020, **8**, 2381.
10 W. Xiang and W. Tress, Review on recent progress of all inorganic metal halide perovskites and solar cells, *Adv. Mater.*, 2019, **31**, 1902851.
11 C. Liu, Q. Zeng and H. Wei, *et al.*, Metal halide perovskite nanocrystal solar cells, progress and challenges, *Small Methods*, 2020, **4**, 2000419.
12 J. D. Deng and J. Xun, *et al.*, Blue-emitting $NH^{4+}$-doped $MAPbBr_3$ perovskite quantum dots with near unity quantum yield and super stability, *Chem. Commun.*, 2020, **56**, 11863–11866.
13 C. Jia, H. Li, X. W. Meng and H. B. Li, $CsPbX_3$/$Cs_4PbX_6$ core/shell perovskite nanocrystals, *Chem. Commun.*, 2018, **54**, 6300–6303.
14 Z. Bao and W. G. Wang, *et al.*, Photo-/electro-luminescence enhancement of $CsPbX_3$ (X = Cl, Br, or I) perovskite quantum dots via thiocyanate surface modification, *J. Mater. Chem. C*, 2020, **8**, 1065–1071.
15 Y. Y. Xu and P. J. Niu, *et al.*, Tailoring multifunctional anions to inhibit methanol absorption on a $CsPbBr_3$ quantum dot surface for highly efficient semi-transparent photovoltaics, *Nanoscale*, 2023, **15**, 9691–9699.
16 P. F. Feng and X. X. Yang, *et al.*, Highly stable perovskite quantum dots modified by europium complex for dual-responsive optical encoding, *ACS Nano*, 2021, **15**, 6266–6275.

17 Z. J. Li and E. Hofman, *et al.*, Photoelectrochemically active and environmentally stable CsPbBr3/TiO2 core/shell nanocrystals, *Adv. Funct. Mater.*, 2018, **28**, 1704288.
18 Q. X. Zhong and M. H. Cao, *et al.*, One-pot synthesis of highly stable $CsPbBr_3$@$SiO_2$ core-shell nanoparticles, *ACS Nano*, 2018, **12**, 8579–8587.
19 L. M. Xu and J. W. Chen, *et al.*, Double-protected all-inorganic perovskite nanocrystals by crystalline matrix and silica for triple-modal anti-counterfeiting codes, *ACS Appl. Mater. Interfaces*, 2017, **9**, 26556–26564.
20 X. W. Li and W. S. Cai, *et al.*, Highly stable $CsPbBr_3$ quantum dots by silica-coating and ligand modification for white light-emitting diodes and visible light communication, *Chem. Eng. J.*, 2021, **419**, 129551.
21 Y. W. Wang and L. Varadi, *et al.*, Spray-assisted coil-Globule transition for scalable preparation of water-resistant $CsPbBr_3$@PMMA perovskite nanospheres with application in live cell imaging, *Small*, 2018, **14**, 1803156.
22 M. A. Mumin, W. Z. Xu and P. A. Charpentier, Quantum dots/silica/polymer nanocomposite films with high visible light transmission and UV shielding properties, *Nanotechnology*, 2015, **26**, 315702.
23 Y. Li, Q. Jun, D. Zhao and R. Song, Preparation of perovskite $CsPb(Br_xI_{1-x})_3$ quantum dots at room temperature, *RSC Adv.*, 2021, **11**(30), 18432–18439.
24 C. Sun, Y. Zhang, C. Ruan, C. Yin, X. Wang, Y. Wang and W. W. Yu, Efficient and stable white LEDs with silica-coated inorganic perovskite quantum dots, *Adv. Mater.*, 2016, **28**, 10088–10094.
25 C. F. Meng, D. D. Yang, Y. Wu, X. J. Zhang, H. B. Zeng and X. M. Li, Synthesis of single $CsPbBr_3$@$SiO_2$ core-shell particles via surface activation, *J. Mater. Chem. C*, 2020, **8**, 17403–17409.
26 B. F. Shi, J. H. Lu, Y. Liu, Y. Xiao and C. L. Lu, Ultra-stable water-dispersive perovskite QDs encapsulated by triple siloxane coupling agent system with different hydrophilic/hydrophobic properties, *Mater. Chem. Front.*, 2021, **5**, 4343–4354.
27 M. Li, X. Zhang and P. Yang, Controlling the growth of a $SiO_2$ coating on hydro phobic $CsPbBr_3$ nanocrystals towards aqueous transfer and high luminescence, *Nanoscale*, 2021, **13**, 3860.
28 J. Song, Y. F. Ren, S. J.Gong, L. Zhao, W. F. Xuan, Z. Lei, Y. L. Zhao, Y. H. Qiang, L. L. Gao and S. Huang, Performance enhancement of crystal silicon solar cell by a $CsPbBr_3$–$Cs_4PbBr_6$ perovskite quantum dot@ZnO/ethylene vinyl acetate copolymer downshifting composite film, *Solar RRL*, 2022, **6**, 2200336.
29 X. Q. Wang, R. Fu, T. Sun, M. Liu, S. Sun, H. Jiang, Z. Li, Y. Zhang, D. Liu, Y. Chen and H. Zhong, Continuously in-situ manufacture of perovskite quantum dots/POE encapsulation adhesive film for silicon solar cell enhancement application, *Sol. Energy Mater. Sol. Cells*, 2023, **259**, 112450.
30 C. Sun, X. Y. Shen and Y. Zhang, *et al.*, Highly luminescent, stable, transparent and f lexible perovskite quantum dot gels towards light-emitting diodes, *Nanotechnology*, 2017, **28**, 365601.
31 K. Hoshi, T. Chiba, J. Sato, Y. Hayashi, Y. Takahashi, H. Ebe, S. Ohisa and J. Kido, Purification of perovskite quantum dots using low-dielectric-constant washing solvent "diglyme" for highly efficient light-emitting devices, *ACS Appl. Mater. Interfaces*, 2018, **10**, 24607–24612.
32 Y. F. Wang, Y. Li, Y. Q. Su, X. R. Chen, R. Wang and J. Y. Xu, *et al.*, Fine purification engineering enables efficient perovskite QLEDs with efficiency exceeding 23%, *ACS Appl. Mater. Interfacess*, 2024, **16**, 28853–28860.
33 T. H. Yang, Z. Zhang, Y. L. Ding, N. Q. Yin and X. L. Liu, Nondestructive purification process for inorganic perovskite quantum dot solar cells, *J. Nanopart. Res.*, 2019, **21**, 101.
34 S. Y. Zhang, J. He and X. Guo, *et al.*, Crystallization dynamic control of perovskite films with suppressed phase transition and reduced defects for highly efficient and stable all-Inorganic perovskite solar cells, *ACS Mater. Lett.*, 2023, **5**, 1497–1505.
35 G. Nedelcu, L. Protesescu and S. Yakunin, *et al.*, Fast anion-exchange in highly luminescent nanocrystals of cesium lead halide perovskites ($CsPbX_3$, X = Cl, Br, I), *Nano Lett.*, 2015, **15**, 5635–5640.
36 A. W. Jansons and J. E. Hutchison, Continuous growth of metal oxide nanocrystals: enhanced control of nanocrystal size and radial dopant distribution, *ACS Nano*, 2016, **10**, 6942–6951.
37 Y. Guo, K. Shoyama, W. Sato, Y. Matsuo, K. Inoue, K. Harano, C. Liu, H. Tanaka and E. Nakamura, Chemical pathways connecting lead(II) iodide and perovskite via polymeric plumbate(II) fiber, *J. Am. Chem. Soc.*, 2015, **137**, 15907–15914.
38 K. Xu, E. T. Vickers and L. S. Rao, *et al.*, Synergistic Surface Passivation of $CH_3NH_3PbBr_3$ Perovskite Quantum Dots with Phosphonic Acid and (3-Aminopropyl)triethoxysilane, *Chem. – Eur. J.*, 2019, **25**, 5014–5021.
39 H. Shan, W. Xuan, Z. Li, D. Hu, X. Gu and S. Huang, Room-temperature hydrogen sulfide sensor based on tributyltin oxide functionalized perovskite $CsPbBr_3$ quantum dots, *ACS Appl. Nano Mater.*, 2022, **5**, 6801–6809.
40 J. Y. Woo, Y. Kim, J. Bae, T. G. Kim, J. W. Kim, D. C. Lee and S. Jeong, Highly stable cesium lead halide perovskite nanocrystals through in situ lead halide inorganic passivation, *Chem. Mater.*, 2017, **29**, 7088–7092.
41 H. Yu, Y. Lu, Z. Feng, Y. Wu, Z. Liu, P. Xia, J. Qian, Y. Chen, L. Liu and K. Cao, A $MAPbBr_3$: poly (ethylene oxide) composite perovskite quantum dot emission layer: enhanced film stability, coverage and device performance, *Nanoscale*, 2019, **11**, 9103–9114.
42 H. Yang, Y. Feng, Z. Tu, K. Su, X. Fan, B. Liu, Z. Shi, Y. Zhang, C. Zhao and B. Zhang, Blue emitting $CsPbBr_3$ perovskite quantum dot inks obtained from sustained release tablets, *Nano Res.*, 2019, **12**, 3129–3134.
43 Y. Li, Y. Lv, Z. Guo, L. Dong, J. Zheng, C. Chai, N. Chen, Y. Lu and C. Chen, One-step preparation of long-term stable and flexible $CsPbBr_3$ perovskite quantum dots/ethylene vinyl acetate copolymer composite films for white light-emitting diodes, *ACS Appl. Mater. Interfaces*, 2018, **10**, 15888–15894.

 

44 C. Liu, Y. Hu, L. Zhang and W. S. Yang, Controllable synthesis of amino-functionalized silica particles via Co-condensation of tetraethoxysilane and (3-Aminopropyl) triethoxysilane, *Langmuir*, 2024, **40**, 25166–25172.
45 Y. H. Chen, S. R. Smock. and A. H. Flintgruber, *et al.*, Surface termination of $CsPbBr_3$ perovskite quantum dots determined by solid-state NMR spectroscopy, *J. Am. Chem. Soc.*, 2020, **142**, 6117–6127.
46 Y. Zhang, X. Liu, Y. Fan, X. Guo, L. Zhou, Y. Lv and J. Lin, One step microwave synthesis of n-doped hydroxyl-functionalized carbon dots with ultra-high fluorescence quantum yields, *Nanoscale*, 2016, **8**, 15281–15287.
47 W. J. Ho, G. Y. Li and J. J. Liu, *et al.*, Photovoltaic performance of textured silicon solar cells with $MAPbBr_3$ perovskite nanophosphors to induce luminescent down-shifting, *Appl. Surf. Sci.*, 2018, **436**, 927–933.
48 M. F. Abdelbar, M. El-Kemary and N. Fukata, Downshifting of highly energetic photons and energy transfer by Mn-doped perovskite $CsPbCl_3$ nanocrystals in hybrid organic/silicon nanostructured solar cells, *Nano Energy*, 2020, **77**, 105163.
49 J. S. Chen, D. Z. Liu, M. J. Al-Marri, L. Nuuttila, H. Lehtivuori and K. B. Zheng, Photo-stability of $CsPbBr_3$ perovskite quantum dots for optoelectronic application, *Sci China Mater.*, 2016, **59**, 719–727.
50 J. Shamsi, A. S. Urban, M. Imarn, L. D. Trizio and L. Manna, Metal halide perovskite nanocrystals: synthesis, post-synthesis modifications, and their optical properties, *Chem. Rev.*, 2019, **119**, 3296–3348.